Calibration of spatially phase-shifted DSPI for measurement of large structures

Babak Saif,[1,*] Bente Hoffmann Eegholm,[2] Marcel Bluth,[2] Perry Greenfield,[1] Warren Hack,[1] Peter Blake,[3] Ritva Keski-Kuha,[3] and Michael North-Morris[4]

[1]Space Telescope Science Institute, Baltimore, Maryland 21218, USA
[2]Swales Aerospace, Beltsville, Maryland 20705, USA
[3]NASA Goddard Space Flight Center, Greenbelt, Maryland 20771, USA
[4]4D Technology, Tucson, Arizona 85706, USA

*Corresponding author: beegholm@stsci.edu

Received 24 January 2007; revised 14 May 2007; accepted 15 May 2007;
posted 15 May 2007 (Doc. ID 79361); published 8 August 2007

We present a method for the calibration of a spatially phase-shifted digital speckle pattern interferometer (SPS–DSPI), which was designed and built for the purpose of testing the James Webb space telescope (JWST) optical structures and related technology development structures. The need to measure dynamic deformations of large, diffuse structures to nanometer accuracy at cryogenic temperature is paramount in the characterization of a large diameter space and terrestrial based telescopes. The techniques described herein apply to any situation, in which high accuracy measurement of diffuse structures are required. The calibration of the instrument is done using a single-crystal silicon gauge. The gauge has four islands of different heights that change in a predictable manner as a function of temperature. The SPS–DSPI is used to measure the relative piston between the islands as the temperature of the gauge is changed. The measurement results are then compared with the theoretical changes in the height of the gauge islands. The maximum deviation of the measured rate of change of the relative piston in nm/K from the expected value is 3.3%. © 2007 Optical Society of America

OCIS codes: 120.0120, 120.6160.

1. Introduction

Digital speckle pattern interferometers (DSPI) or electronic speckle pattern interferometers (ESPI) have been used for measurements of diffuse objects in experimental mechanics since early 1970s. Depending on the measurement configuration, in-plane or out-of-plane deformation and the displacement of the test article can be measured. In the 1980s the accuracy of the ESPI measurements were tremendously improved by incorporating temporal phase shifting [1]. Temporal phase shifting directly facilitated the extraction of quantitative data from the measurements by providing sufficient information in the form of phase-shifted interference patterns to solve for the phase. The drawback to temporal phase shifting is that it requires capturing three or more frames of data sequentially in time, which makes the measurement susceptible to vibrations. Typically, it takes 150 ms to collect the measurement frames. Movements in the test article during this period of time result in a measurement error or a complete washout of the interference pattern, which makes it virtually impossible to measure large test articles. In the early 1990s the phase shifting of ESPI measurements was extended to the realm of spatial phase-shifting by the spatial carrier method, which significantly reduces the vulnerability of phase-shifted measurements to vibration [2]. The SPS–DSPI characterized in this paper captures all the phase-shifted frames required to extract the phase in 9 ns, which is eight orders of magnitude faster than temporal phase-shifting methods, using a pixelated phase mask. In this paper we are reporting on the calibration of a SPS–DSPI [3]. The SPS–DSPI was developed to measure the James Webb Space Telescope (JWST) optical support structures and related technology development structures

0003-6935/07/235622-09$15.00/0
© 2007 Optical Society of America

to nanometer accuracy [4–6]. One example is the 6.5 m, lightweighted, cryogenic, diffuse back plane, which holds the 18 segments that comprise the primary mirror.

Testing diffuse structures to nanometer accuracy is relevant not only for aerospace, but also for other applications. The principles and requirements of a SPS–DSPI with the capability to test large, diffuse structures was conceived in the JWST project. The instrument building expertise and unique simultaneous pixelated spatially phase-shifting technique was found at 4D Technology (Tucson, Az) [7], who manufactured the instrument and subsequently has made it commercially available under the name SpeckleCam 5100. For our particular test purposes where testing is planned to take place over several weeks, and where the test environment requires a continuous series of measurements taken with short intervals (on the order of five measurements per second), a considerable amount of software was custom developed for the instrument by the JWST project.

The calibration of the instrument is done using a single-crystal silicon gauge [8]. The gauge has four islands of different heights that change in a predictable manner as a function of temperature. The SPS–DSPI is used to measure the relative piston between the islands as the temperature of the gauge is changed. The measurement results are then compared with the theoretical changes in the height of the gauge islands. Since the changes in the gauge step-heights are governed by the physics of the crystal structure, they are extremely predictable and tie the calibration of the SPS–DSPI to a well characterized standard. By calibration, in this context, we mean determining the accuracy of the interferometer.

2. Spatially Phase-Shifted–DSPI Interferometer

DSPI is a well-known technique for measuring deformations of diffuse objects under stress. The DSPI discussed in this paper uses the simultaneous phase-shifting technique, where four 90° phase-shifted interferograms are captured simultaneously in a single image. This enables us to obtain accurate measurements in the presence of vibration. This, what we believe to be a newly developed interferometer, combines the classical speckle pattern interferometer for measurements of out-of-plane motions with a spatially phase-shifted interferometer [3,7].

This interferometer incorporates a pixelated phase mask that encodes the required phase shifts on the camera image on a pixel-by-pixel basis. Parsing the images results in four phase-shifted interference patterns. It is configured to measure the out-of-plane deformation and displacements of large articles at cryogenic temperatures. Figure 1 shows a schematic block diagram of the interferometer. The object under test is illuminated with a high power pulsed Nd:YAG laser, which operates at the second harmonic (532 nm). The laser is seeded to keep it in a single mode. After seeding and doubling, the maximum energy output per pulse is about 0.9 J. The pulse duration is 9 ns and the pulse repetition rate is 10 Hz, which sets

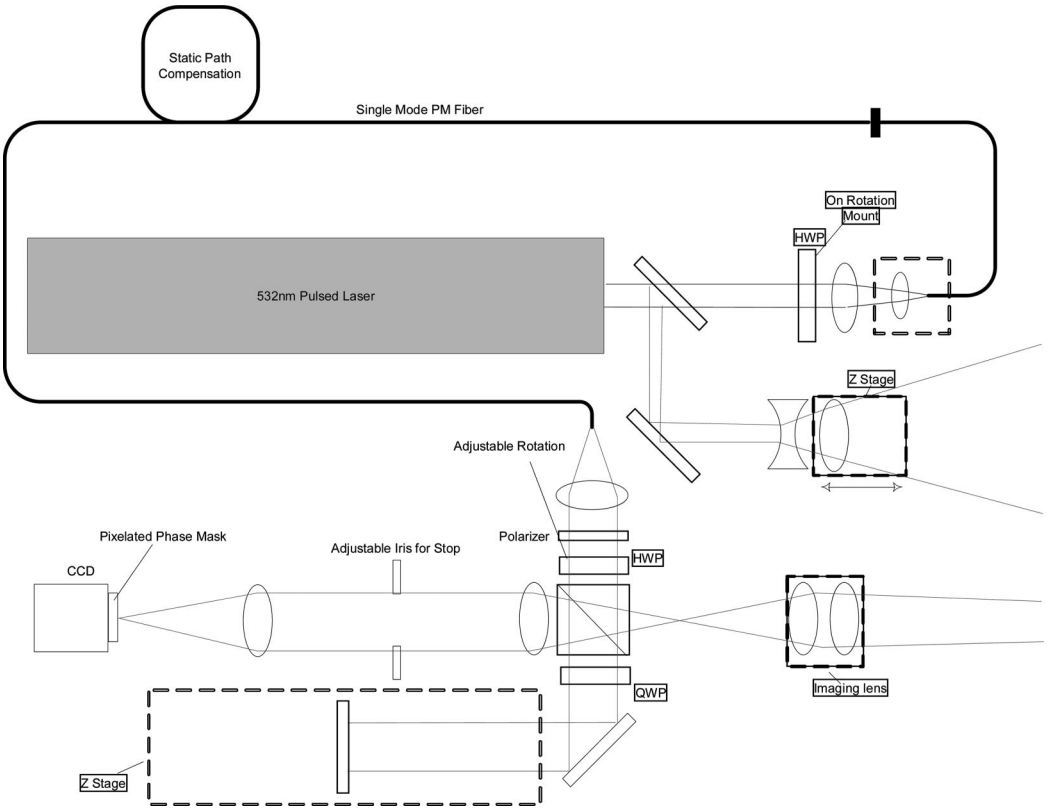

Fig. 1. Schematic block diagram of the SPS-DSPI.

the upper boundary of the SPS–DPSI measurement rate. The coherence length of the laser is about 3 m. In the interferometer front-end the laser light is split into two beams. The majority of the energy illuminates the test article, and a small fraction of the energy is coupled into a single mode, polarization maintaining photonic crystal fiber. The signal in the fiber is routed into the interferometer and serves as the reference. The length of the fiber is chosen to match the optical path of the test and reference signals, so that both pulses arrive at the camera at the same time.

The reference beam emanating from the fiber is collimated and passes through a half-wave plate and a polarizer plate before being directed onto the camera via a polarizing beam splitter by way of an imaging relay. This half-wave plate enables the operator to adjust the energy balance between the reference and the test beams. The stop in the imaging relay controls the optical throughput and the speckle size on the camera. Due to the lateral offset of the phase-shifted samples, the smallest size of the speckle diameter that will provide a reasonable noise floor is about 25 μm. The limit on the speckle diameter places an inherent limit on the throughput of the imaging path.

The test beam is directed onto the test article via an illumination module that controls the distribution of the irradiance impinging on the test article, and allows the illumination to be directed to different locations on the test article. The illumination zoom was designed to illuminate a 3 m test article at a 16 m distance, and can be zoomed down to illuminate a 2 m diameter portion of the same test article.

Three interchangeable imaging lenses are supplied with the interferometer and are used one at a time. The imaging lenses are designed to image a 3 m (1× lens), 1 m (3× lens), and 0.5 m (6× lens) structure at a 16 m distance. These lenses form an intermediate image inside the interferometer. The intermediate image is relayed by a $f/4$ lens system back to the CCD. At the Fourier plane of the $f/4$ system there is an aperture, which enables us to change the speckle size. The $f/4$ system consists of two identical lenses configured to collimating a point source and imaging it. The system is telecentric in object and image domain. The CCD has 1000 × 1000 pixels, and the pixelated phase mask is attached to it directly [7].

The interferometer is also equipped with a p-i-n diode, which can be flipped into the optical path to facilitate the process of ensuring that the pulses from the reference and the test beams overlap sufficiently in the time domain. With the appropriate fiber length inserted in the reference path, the overlapping is done in two stages: coarse, by moving the interferometer as a rigid body in the direction of the optical path and, fine, by adjusting an optical delay line inside the interferometer. The optical delay line is a flat mirror on a carriage, which changes the optical path of the reference beam by up to +/−0.5 m. To acquire good contrast fringes, the overlap cannot be off more than 2 ns, which corresponds to less than 25% of the laser pulse width. In addition, good contrast fringes require that the beam ratio (reference energy/energy returned from the object under test) is maintained at about 20.

3. Spatially Phase-Shifted–DSPI Set Up Parameters

The SPS–DSPI interferometer measures the change between the states of an object under stress. First, a measurement of the object is made to create the reference object interferogram. The object interferogram is the interference pattern that results from interfering the object beam (speckled) and the reference beam. Next, the object under test is subjected to a thermal and/or mechanical stress. The modified object interferogram is created. Using the eight intensities from the four phase-shifted interferograms in each measurement, the wrapped phase difference between the two states is calculated. The four measured interferogram intensity patterns I_1, I_2, I_3, and I_4 are used to detect each wavefront phase. The intensity bias term is eliminated by subtracting the equations in pairs, so that

$$\tan \phi_i = (I_{i,4} - I_{i,2})/(I_{i,1} - I_{i,3}), \tag{1}$$

$$\tan \phi_f = (I_{f,4} - I_{f,2})/(I_{f,1} - I_{f,3}), \tag{2}$$

where ϕ_i and ϕ_f are the phases of the object interferogram and the modified object interferogram. I_i is the initial object intensity, and I_f is the modified, final object intensity; $I_{i,1}$ and $I_{f,1}$ are object and modified object interferograms with a zero phase shift; $I_{i,2}$ and $I_{f,2}$ are object and modified object interferograms with a $\pi/2$ phase shift; $I_{i,3}$ and $I_{f,3}$ are object and modified object with π phase shift; and $I_{i,4}$ and $I_{f,4}$ are object and modified object interferograms with $3\pi/2$ phase shift.

$$\tan(\phi_i - \phi_f) = (\tan \phi_i - \tan \phi_f)/(1 + \tan \phi_i \tan \phi_f), \tag{3}$$

$$\tan(\phi_i - \phi_f) = \frac{(I_{i,4} - I_{i,2})(I_{f,1} - I_{f,3}) - (I_{f,4} - I_{f,2})(I_{i,1} - I_{i,3})}{(I_{i,1} - I_{i,3})(I_{f,1} - I_{f,3}) + (I_{i,4} - I_{i,2})(I_{f,4} - I_{f,2})}. \tag{4}$$

The spatial smoothing is performed as an initial step in calculating the wrapped phase. In spatial smoothing, an averaging moving window is applied to the numerator and denominator of the arctan function independently. This spatial smoothing reduces the speckle noise, however, at the expense of a reduced spatial resolution. A windowing of 9 × 9 pixels is used in our measurements, i.e., $n = 9$ in (5).

When spatial smoothing is done over the n neighboring points, the wrapped phase difference between the two states can be written as [3]

$$\phi_f - \phi_i = \arctan\left[\frac{\sum_n (\Delta I_{f42n}\Delta I_{i13n}) - (\Delta I_{f13n}\Delta I_{i42n})}{\sum_n (\Delta I_{f13n}\Delta I_{i13n} + \Delta I_{f42n}\Delta I_{i42n})}\right], \tag{5}$$

where

$$\Delta I_{f42} = I_{f,4} - I_{f,2}, \text{ etc.}$$

4. Calibration Reference Article

To characterize the relative accuracy of our interferometer in the nanometer regime a single crystal silicon gauge, hereafter called the calibration reference article (CRA) was developed. This allows us to measure the deformation of a material with well-known and uniform behavior. A temperature change is applied as a stimulus to introduce a well-defined deformation in the material.

The CRA is shown in Fig. 2. It has four islands; the height difference between the two high islands is 4 mm, and the height difference between the two low islands is 2 mm. The lowest and the highest island are 63 mm apart. The gauge is 8 in. in diameter.

The SPS–DSPI was placed at ambient temperature, about 30 cm away from the vacuum chamber window. The CRA is placed inside the chamber, 15.1 m away from the SPS–DSPI. The distance is chosen to be the same as the planned distance to the large structure, which subsequently will be tested. The calibration is performed in vacuum, which will also be applied for the large structure cryogenics test. The calibration is performed in the same geometric test setup as the subsequent test of the large structure. The chamber was evacuated and the CRA was locally heated over the range from 290 K to about 300 K. The duration of each measurement was 1 h. Measurement of the change in the relative piston between the islands is made through the chamber window, which is an 8-in. diameter window optimized for minimum reflection (0.1%) at 532 nm. Relative piston as a function of temperature is plotted and compared to the expected values based on the well-known coefficient of thermal expansion (CTE) of silicon. Over the range of temperatures of interest, 250 to 300 K, the CTE of the material is $2.55 \times 10^{-6}\,\mathrm{K}^{-1}$. The CTE predictions are based on a model [8], which predicts the CTE to an average uncertainty of $70 \times 10^{-9}\,\mathrm{K}^{-1}$ in the ambient temperature range from 250 to 300 K, and the rate of change of relative piston is obtained by simply multiplying the design height difference between the islands with the CTE.

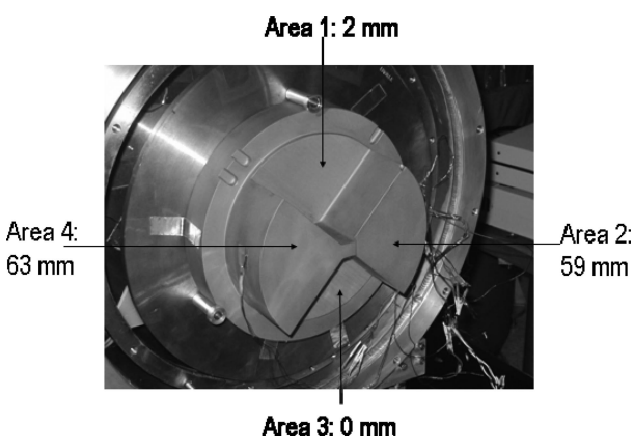

Fig. 2. CRA mounted on a copper plate: area 1 has a height of 2 mm, area 2 has a height of 59 mm, and area 4 has a height of 63 mm with respect to area 3. The diameter of structure is 8 in. The material is single crystal silicon with well-defined and uniform CTE, 2.55×10^{-6}, at ambient temperature.

The strategy for designing the CRA was to enable a measurement of a extremely predictable deformation as a function of temperature. The high predictability is achieved by selecting a single crystal silicon piece, and a machine to have four islands of different heights along the optical axis of the SPS–DSPI. The relative piston between the islands, i.e., deformation, in the out-of-plane direction seen from the SPS–DSPI can be measured as a function of temperature. The CRA is designed with the highest and the lowest of the islands with a height difference yielding a relative piston at ambient temperature at the same order of magnitude as the deformation at 30 K expected from the ultimate JWST structure to be cryotested with the SPS–DSPI after the calibration. The two lowest islands as well as the two highest islands on the CRA are designed with a smaller height difference in order to enable measurement of the resolution.

The exact shape of a CRA and the number of islands is dependent on the test situation, but for an instrument, such as the SPS–DSPI, which measures out-of-plane deformation, it is important to align the piston direction with the optical axis of the instrument. The size of the islands should be chosen in accordance with the optical system, so that enough pixels on the CCD are being illuminated, for signal to noise reasons.

The measurements are performed with the 1×, 3×, and 6× imaging lenses.

5. Decorrelation

In speckle interferometry, the accuracy of the measurement is directly related to the decorrelation of the speckle pattern before and after stress is applied. The decorrelations are due to decentrations, tilts, and deformation of the article between the two states. Decentrations shift the speckle pattern at the CCD. The tilt of the object results in angular decorrelation, which is more serious, because the speckle pattern is rewritten at the CCD. Experiments were conducted to measure the acceptable amount of tilt due to angular decorrelation. In order to maintain an accuracy of less than 10 nm RMS, the acceptable tilt of the object for our system is 42 pixels per fringe. The dynamic range of the same interferometer is 12 pixels per fringe.

In the characterization of optical structures, where the dynamic deformation is of interest, it is necessary to measure the article under test over a period of time. Dependent on the test, this time period is typically days or weeks. The reference object interferogram—also known as the baseline—can be used for a number of measurements. To minimize decorrelation of speckle patterns, the baseline needs to be changed over time. Changing the baseline is called rebaselining. The angular decorrelation is used as one of the criteria for

changing the baseline. It was used when we were not pixel starved, which was the case for the 6× imaging lens. But due to lack of pixels, in the case of using the 3× and 1× imaging lens, respectively, other decorrelation factors, such as print-through noise, effected the measurements. In such cases rebaselining was done to minimize decorrelations due to these noises.

Rebaselining entails selecting a new, more recent, interferogram for use as baseline. It is assumed in the data analysis that during a baseline interval, the relative piston does not change more than a wavelength. This is a valid assumption, since it is possible to predict the change to much less than a wavelength, and a change of more than a wave is readily apparent in the data.

Algorithms for optimizing the rate of rebaselining is part of the software developed for the SPS–DSPI. Any interferogram measurement can be used as a baseline, and by storing all measurements in a measurement series, the rebaselining can be changed in the data analysis process after the measurement series is completed, which enables optimization of the measurement performance.

The repeatability of the SPS–DSPI is 2.1 nm. The method for determining the repeatability is as follows: while no stress is applied to the CRA, the relative piston between the highest and the lowest island is measured ten times in rapid succession. The average and the RMS of these ten measurements are calculated. Next, a new set of ten measurements is taken, and the average and RMS are calculated. This process is repeated, until a total of 15 sets of ten measurements are taken. The repeatability is defined as the RMS of the 15 RMSs, corresponding to the definition used by the manufacturer.

6. Relative Piston Measurements Using SPS–DSPI

Our interest is to measure the relative piston between surfaces that are discontinuous (islands), as this directly applies to the large diffuse JWST structures, for which the SPS–DSPI instrument was developed. A segmented detector mask is applied to our segmented object, the CRA. Once the smoothed wrapped phase is acquired, the spatial phase unwrapper is applied to each island individually. The result of the unwrapper is island surfaces. The island with the largest number of pixels is chosen as the reference island. Rigid body motion and tilt is removed from that island. In effect, all other islands are rotated to a coordinate system in which the reference island is flat (i.e., shows no tilt). Next, all the islands are leveled with respect to the reference island. Leveling means adding an integer number of half-wavelengths to the piston value reported by the unwrapper for each island, in order to get each island within plus or minus one-quarter of a wavelength from the reference island.

This process is repeated for each exposure. The relative piston motion is plotted against the stimulus, which is temperature in our case. In this measurement series of the CRA the rebaselining took place before the piston wrapping, so there was no need to unwrap the piston within a baseline. In this reported measurement setup, rigid body tilt of the CRA was much larger than the relative piston (deformation). If, however, the relative pistons (deformations) were much larger than the rigid body motion, the pistons would have to be unwrapped within a baseline.

7. Data Acquisition and Software

The data acquisition and software algorithms are optimized with the purpose of conducting dynamic deformation measurements on large optical structures and related technology development structures for JWST. As these types of tests typically take several weeks of continuous round-the-clock data taking, because a number of cooling cycles have to be performed, a high capacity computer system is required for collecting, storing and processing the SPS–DSPI measurements. The data-taking rate is five measurements per second. A real-time monitoring capability allows the test personnel to monitor the progress in the test results and the performance of SPS–DSPI instrument and laser in terms of fringe quality and beam ratio. Since every measurement is stored, it is always possible to reprocess the data using a different algorithm or a different rebaselining period, if so desired.

Data acquisition and spatial phase unwrapping routines available within 4D Technology's 4Sight application were used, and a substantial amount of custom additional software was written in Python language to:

- Increase the image capture rate to (five images/second),
- Maximize the data acquisition and processing throughput and manage the data files,
- Construct detector, unwrapping, and analysis masks,
- Provide monitoring functions so that operators could monitor data quality and be warned of abnormal conditions,
- Apply different rebaselining criteria,
- Apply custom phase processing algorithms, and
- Allow unattended reprocessing of the data using different parameters.

The masks used for the measurements are derived from NASTRAN Finite Element Models for the structure front surface. The tool is developed to accommodate the JWST structure to be tested, but is general in nature because of the way it enables masking of specific complex geometric structures under test. The software is used to determine the outlines of the front surfaces by eliminating all nodes on the interior or edges of the surface and only retaining the vertices. The polygons so generated are then appropriately geometrically transformed from the NASTRAN coordinate system to the image coordinate system (i.e., to pixel coordinates). The coordinate transformation is determined by iteratively adjusting the transformation parameters manually until a plot of polygons matches the image obtained of the structure to be tested. A geometric distortion model, as provided by

4D technology for their imaging system, is applied to the transformed coordinates before plotting.

The transformation parameters, along with the model polygons and distortion model, are used to derive the mask images used for processing. The raw mask in effect grows the island models to provide sufficient boundaries to ensure that no data are lost due to possible shifts in the target image over time. The spatial mask is what is used to do the spatial phase unwrapping. It corresponds most closely with the outline of the polygon models. The analysis mask is a shrunken version of the polygon model. This is to ensure that the phases used in the analysis of any given island are not contaminated by phase values in other islands due to the 9×9 pixel smoothing used to increase the signal to noise.

8. Data Processing

SPS–ESPI measurements were taken of the CRA using several different imaging lenses and temperature conditions. These data consisted of raw exposures taken at a rate of five exposures per second, with each exposure containing only the raw phase information after masking out all nontarget areas of the field of view. Processing these data requires setting a baseline which serves as the zero-point for the phase difference with each subsequent exposure. This baseline needs to be redefined multiple times during the test in order to avoid decorrelation of the phases, and in our case, fixed baseline periods were defined for the processing. This fixed period is shorter than the angular decorrelation period by a factor of 3.

The flow chart of the CRA processing software is shown in Fig. 3. The processing takes place in the processing computer, which through a fast local network receives the raw data acquired in each SPS–DSPI exposure.

The processing of this data consists of several steps; namely,

- Convert each raw exposure to a phase.
- Calculate the phase difference between the new phase and the baseline phase.
- Unwrap the phase, using the exclusion mask, a.k.a. the detector mask.
- Remove the tilt:
  (a) A fit plane is fitted to the selected CRA reference island.
  (b) The fit plane is subtracted from all four CRA islands.
  (c) Check whether baseline criterion is met. If not, the most recent exposure is selected as new baseline, and a reprocessing is performed.
  (d) Level all islands (move all islands to $+/-\lambda/4$ of the reference island).
  (e) Measure the average relative piston of each defined island.
- A slope (nm/K) is fitted to the data in each baseline period.
- A weighted mean slope is computed.

The data in each baseline is fit using a simple linear regression to compute a single slope of displacement over temperature for that baseline period. This fit starts with the matrix equation:

$$R = M * v, \tag{6}$$

where M and R are defined as

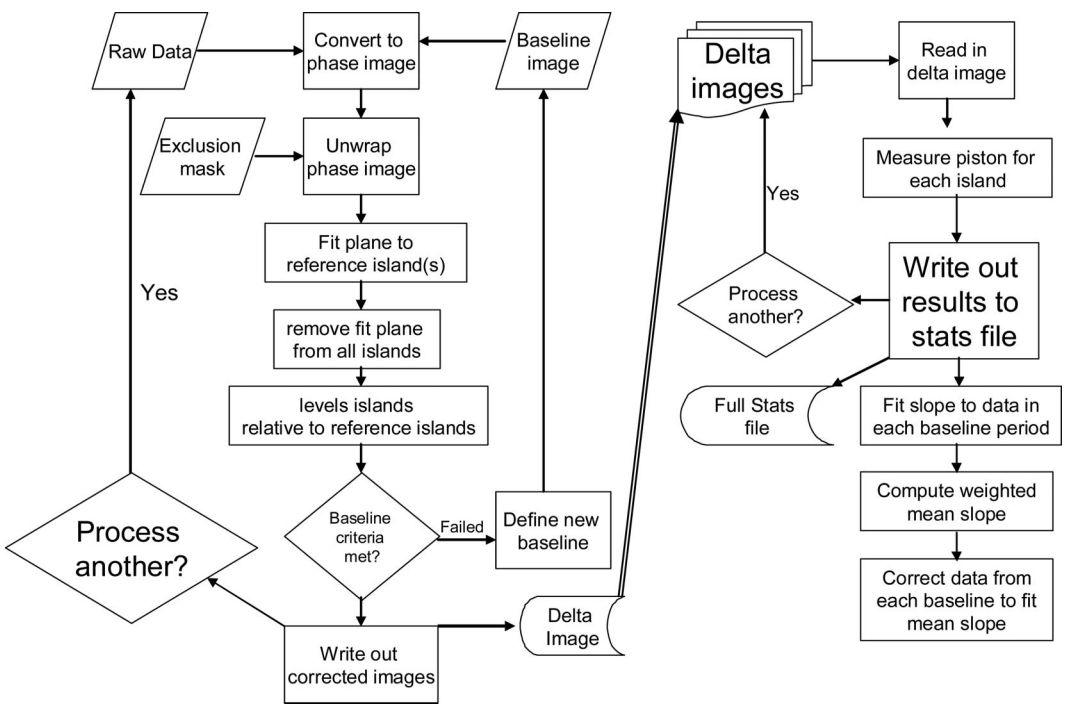

Fig. 3. Flow chart for the software for processing CRA data. The baseline criteria used is a fixed time interval.

$$M = \begin{bmatrix} \sum x_i^2 & \sum x_i \\ \sum x_i & n \end{bmatrix}, \tag{7}$$

$$R = \begin{bmatrix} \sum (y_i * x_i) \\ \sum y_i \end{bmatrix}, \tag{8}$$

for all "n" points "i" in each array.

In our case, x is the temperature at each measurement, and y is the displacement relative to the reference baseline for the period. The solution to this returns the slope, m_0, the zero point, y_0, and the sigma, m_σ, for each baseline period. These slope and zero-point values are used to compute the residuals for each point in the baseline period:

$$\text{resid} = y - (m_0 * x + y_0). \tag{9}$$

The sigma, m_σ, gets computed as:

$$m_\sigma = M^{-1} * (\text{stddev}(\text{resid})^2), \tag{10}$$

where M is the linear matrix defined earlier, and the "stddev( )" function computes the standard deviation of the distribution of residuals. This takes into account the number of points in each baseline period, through the inverse of the linear matrix, while also folding in the scatter of the input data through the use of the residuals.

An initial clipping of bad slopes gets performed by deleting any slope which had a residual three times the standard deviation of the residuals. This clipped set of slopes, along with the corresponding standard deviation of the residuals for each those slopes, is then used to compute the overall slope. A weighted average slope subsequently gets computed using the slopes from each baseline and its associated weight, m_σ, using:

$$\text{mean_slope} = \frac{\sum \left(\frac{\text{slopes}_j}{m_{\sigma j}} \right)}{\sum \left(\frac{1}{m_{\sigma j}} \right)}, \tag{11}$$

where the sum is over all the values of the slope and m_σ for all "j" baseline periods. The weights are separated from the predictions of the slope.

Figure 4 shows the raw data for measurement of the relative piston between the highest and the lowest CRA islands. The x axis shows the temperature in K, the y axis shows the relative piston in nm. The characteristic periodic, saw-tooth shape of the data arises from the fact that rebaselining is applied during data taking.

The relative piston was measured between the highest and the lowest island on the CRA as a function of temperature. Figure 5 shows an excerpt of the raw measurements, for a long baseline period of 7 min. The dots represent measured relative piston, the dashed line shows the fitted slope using all the relative piston measurements. The solid line shows the fitted slope excluding the relative measurements during the "bulge" period. Figure 5 clearly shows that the scatter changes during the baseline period.

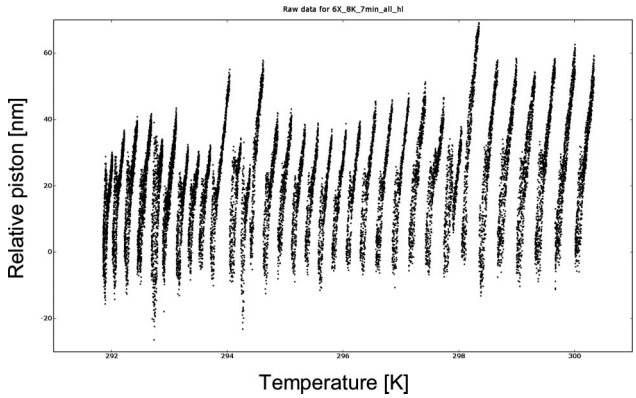

Fig. 4. Raw data plot. The y axis shows the relative piston in nm between the highest and the lowest CRA islands as a function of temperature, which is changed from 292 to 300 K. The 6× imaging lens is used.

Examination of raw measurements for a long baseline period (Fig. 5) demonstrates the types of errors which need to be addressed in this analysis. The scatter of the data along the fit can be seen to cover three regimes. The initial period in the baseline corresponds to measurements which demonstrate very little rigid body motion (tilt) allowing for clean measurements of the relative piston. However, as the tilt increases, print-through noise results in errors in the tilt computation. The inherent noise from the phase shifting is apparent as print-through noise when only a low number of fringes are measured across the structure. For zero fringes, there is no print-through. This is also the case when many fringes are measured across the structure, as the noise averages out. The optimal rebaselining intervals were determined by taking the print-through noise phenomenon into account. These tilt computation errors subside as the tilt increases and print-

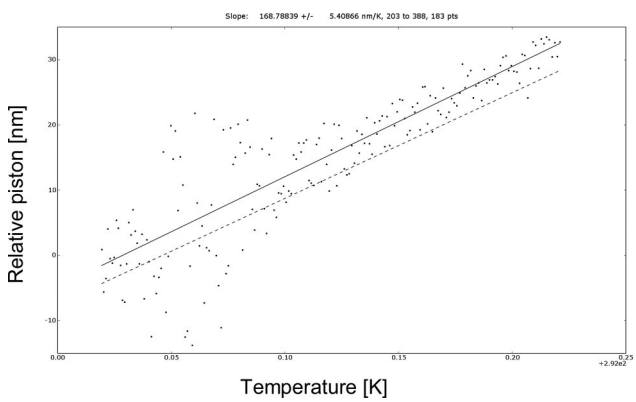

Fig. 5. Relative piston between the highest and the lowest islands on the CRA as a function of temperature. Excerpt of the raw measurements, for a long baseline period of 7 min. The dots represent measured relative piston, the dashed line shows the fitted slope using all the relative piston measurements. The solid line shows the fitted slope excluding the relative measurements during the bulge period. The scatter changes during the baseline period.

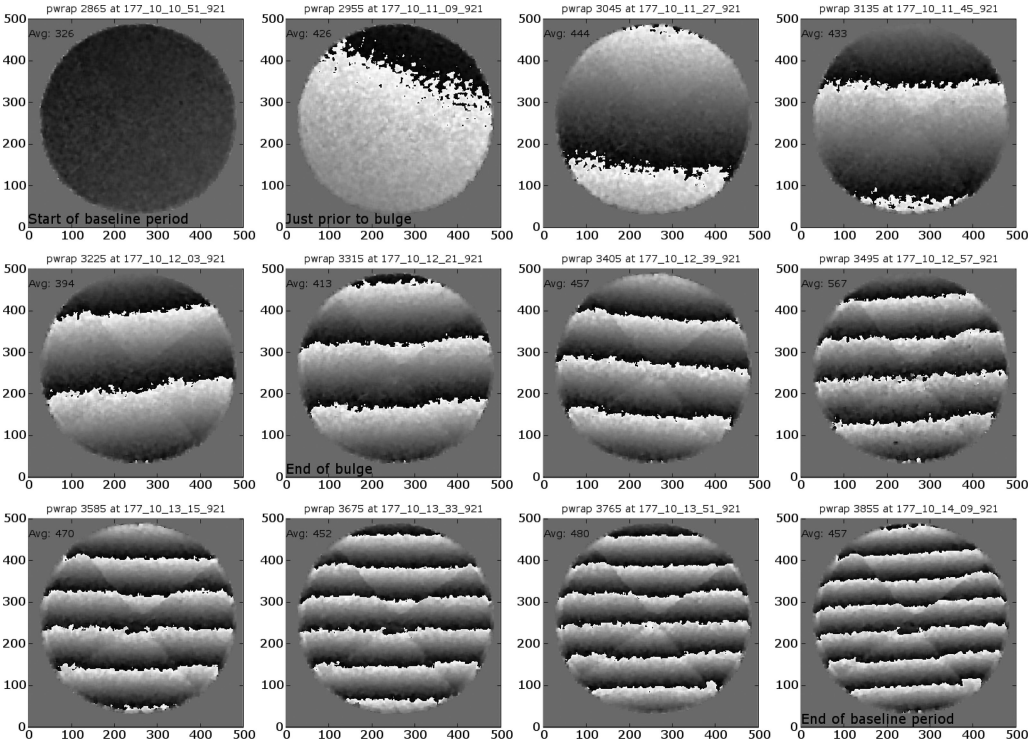

Fig. 6. Fringe mosaic for a baseline period (7 min start to end). The size of each of the figures is 500 pixels wide × 500 pixels high. The pictures are numbered left to right, top to bottom. The bulge period starts at picture 2 and ends at picture 6. The correlation in time is seen between the bulge in the raw data plot and the low number of fringes on the CRA.

through noise gets averaged out. This led us to select short baseline periods which would not only avoid decorrelation effects, but also errors in the tilt correction. For the 6× data, this is not so much of a problem as there are enough pixels to compute the tilt to avoid significantly skewing the results. However, for the 3× data and 1× data, we found that these shorter baselines avoided bias from these errors and produced slopes which were only off from the model by only 3%. Basically, as the number of pixels on the CRA islands decreased, a shorter baseline period was required to accurately measure the changes in step height as the temperatures changed.

Whereas for imaging lenses 3× and 1× it was necessary to select short baseline periods, this was not necessary for 6× because of the higher number of pixels. Figure 6 is a fringe mosaic for a measurement series on the CRA taken with the 6× lens and a long baseline period of 7 min. The annotation on the fringe pattern denotes to which event in the baseline period a fringe pattern is attributed. The time period where the number of fringes is low is attributed to the time period of the bulge in the raw data plot. The mosaic plot illustrates how tilt builds up, and shows the

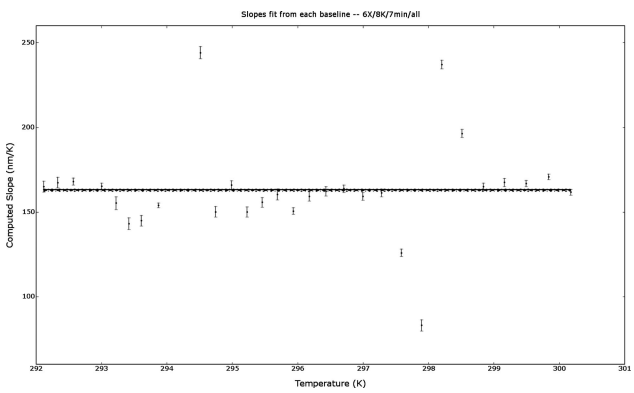

Fig. 7. Slope plot for 6× lens measurement at 15.1 m distance from SPS–DSPI. Rebaselining is done every 7 min. The resulting relative piston between the island surfaces of the CRA can be found from integration of the relative piston change over the temperature interval. The mean slope is shown as the dotted line, the expected slope from the model is shown as the solid line.

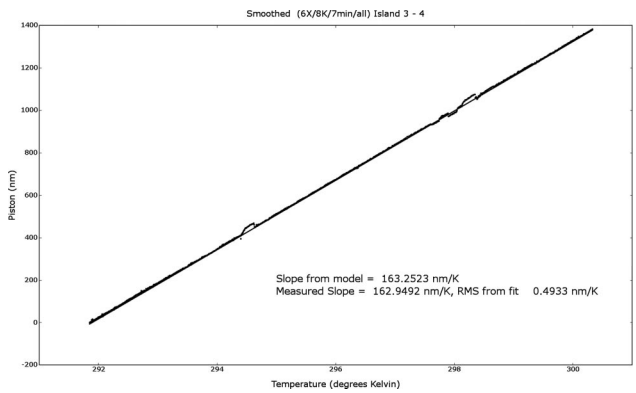

Fig. 8. Calibration results obtained with the 6× lens at 15.1 m distance, in vacuum. The relative piston between the highest and the lowest island was measured.

Table 1. List of Calibration Measurements Performed on the CRA in Vacuum, at 15.1 m away from the SPS–DSPI[a]

Lens	Expected Slope (nm/K)	Temperature Change (h)	Rebaselining Period (min)	Islands (#)	Pixels per Island (#)	Slope (nm/K)	RMS (nm/K)	Deviation from Exp. Slope (%)
6×	10.77	8 K	3	Hi-Hi	27,154	10.67	+/−0.80	0.93
6×	163.25	8 K	7	Hi-Lo	27,154	162.95	+/−0.49	0.18
3×	162.02	3 K	3	Hi-Lo	4,825	167.28	+/−3.40	3.25
1×	162.06	3 K	0.5	Hi-Lo	625	166.90	+/−5.54	2.91

[a]The measurements were taken over duration of 1 h, with the temperature changed from ambient.

excess noise in the beginning of the period. For the 6× measurement in Fig. 6, the number of tilt fringes builds up between rebaselinings, but the angular correlation is honored, because the last exposure before rebaselining yields 60 pixels per fringe, which exceeds the 42 pixels per fringe correlation criteria.

Figure 7 shows the slope of the relative piston curve for each baseline as a function of temperature change in nm/K. Each point on the plot is the slope of the relative piston [nm] as a function of temperature [K] for each baseline period. The mean slope [Eq. (11)] in [nm/K] is reported as the result of the previously explained statistical analysis of the slopes for each individual baseline. The mean slope is 162.95 nm/K +/−0.49 nm/K. The expected value from the model is 163.25 nm/K.

9. Results

In the following, we report the CRA measurement results for the 6×, 3×, and 1× lenses. The relative piston is plotted as a function of the temperature. The number of pixels in each island on the CRA is dependent on the imaging lens used. For the 6× lens, the number of pixels per island is 27,154. For the 3× lens, the number of pixels per island is 4825. For the 1 × lens, the number of pixels per island is 625.

Figure 8 shows a CRA measurement with the 6× lens, where the CRA temperature is changed 8 K from 292 to 300 K. The relative piston between the highest and the lowest island was measured. The dots show binned measurements, each dot showing an average of 16 consecutive measurements. The solid line denotes the expected curve with a slope of 162.25 nm/K. The measured slope is 162.95 nm/K +/−0.49 nm/K.

Next, the relative piston between the two highest islands was measured, and subsequently the CRA measurements of the relative piston between the highest and the lowest island were performed also with the 3× and 1× imaging lenses. The results are summarized in Table 1. The measurements were taken over duration of 1 h each, with the temperature change from ambient. In all cases the CRA was placed inside the chamber, in vacuum, and 15.1 m away from the SPS–DSPI, which was placed outside the chamber. The slope is found as the slope of the linear fit to the relative piston measurements. The RMS is the RMS from the linear fit of the relative piston measurements.

10. Conclusion

We have characterized this new spatially phase-shifted digital spackle pattern interferometer (SPS–DSPI) using a single crystal silicon gauge. The results of the calibration of this new DSPI shows repeatability of 2.1 nm RMS.

In addition, the deviation of the measured slopes from the expected ones, in nm/K, are between 0.5% and 3.3% with RMSs of 0.5 nm/K to 5.5 nm/K, dependent on the imaging lens. The larger RMSs for the 1× lens data are attributed to the smaller number of pixels. Measuring the relative piston of different islands and different slopes shows that this relative accuracy does not strongly depend on the slope value. These results are important in the subsequent cryogenic tests of the large, diffuse structures for JWST, in which the SPS–DSPI is the key instrument.

We gratefully acknowledge the staff at the NASA Marshall Space Flight Center X-Ray Calibration Facility for their contribution to this work: Ron Eng, Jeff Kegley, Harlan Haight, William Hogue, Mark Baker, Ernie Wright, Richard Siler, John Tucker, Jay Carpenter, Tom Kester, and Joe Geary, University of Alabama.

References

1. K. Creath, "Phase-shifting speckle interferometry," Appl. Opt. **24,** pp. 3053–3058 (1985).
2. H. Steinbichler and J. Gutjahr, U.S. Patent No. 5,155,363A (1990).
3. B. Saif, "Simultaneous phase-shifted digital speckle pattern interferometry," Ph.D. dissertation (University of Arizona, 2004).
4. P. Sabelhaus and J. Decker, "An overview of the James Webb space telescope (JWST) project," Proc. SPIE **5487,** 550–563 (2004).
5. C. Atkinson, S. Texter, R. Hellekson, K. Patton, R. Keski-Kuha, and L. Feinberg, "Status of the JWST optical telescope element," Proc. SPIE **6265,** 62650T (2006).
6. J. Arenberg, L. Gilman, N. Abbruzze, J. Reuter, K. Anderson, J. Jahic, J. Yacoub, H. Padilla, C. Atkinson, D. Moon, K. Patton, P. May, J. York, T. Messer, S. Backovsky, J. Tucker, C. Harvey, M. Bluth, B. Eegholm, B. Zukowski, B. Saif, R. Keski-Kuha, P. Blake, J. Kegley, and K. Russell, "The JWST backplane stability test article: a critical technology demonstration," Proc. SPIE **6265,** 62650Q (2006).
7. M. N. Morris, J. Millerd, N. Brock, J. Hayes, and B. Saif, "Dynamic phase-shifting electronic speckle pattern interferometer," in *Optical Manufacturing and Testing VI,* H. P. Stahl, ed., Proc. SPIE **5869,** 58691B (2005).
8. M. Bluth, "CTE Model," SAI-TM-2865, Technical memorandum, not published (2005).